30th NENE 2021 September 6 - 9 BLED-SLOVENIA
International Conference Nuclear Energy for New Europe

Numerical Simulation of Melt Droplet - Water Interaction in Steam Explosions

Nikita Sivakov, Sergey Yakush
Ishlinsky Institute for Problems in Mechanics RAS
101/1 Vernadsky Ave.
119526, Moscow, Russia
sivakov-nikita.ru@yandex.ru, yakush@ipmnet.ru

ABSTRACT

Numerical studies by the volume of fluid (VOF) method are performed for the interaction of hot melt droplet with water initiated by the arrival of a pressure pulse in the ambient water. The shapes of the melt surface and vapor film, as well as the time histories on the volume of vapor in the film are obtained in the parametric studies where the ambient pressure pulse maximum pressure, the growth and decay times were varied. Numerical simulations were performed for a 7.32 mm diameter molten tin droplet at the initial temperature 950 K, immersed in subcooled water with the temperature of 353 K, the initial pressure was 1 bar, the peak pressure was 40 and 80 bar. One to three cycles of vapor film collapse and growth are obtained in the simulations, which is consistent with experimental observations on single droplet steam explosions reported in the literature. Simulations confirmed that impact of water jets on the melt surface can disturb the droplet surface significantly. The simulations emphasize the importance of taking into account the shape of the triggering pressure pulse which can affect the number of vapor bubble oscillations, as well as the melt disturbances and fragmentation.

1 INTRODUCTION

Steam explosions occurring when a high-temperature melt contacts with water or other coolant with the boiling temperature lower than the temperature of the molten material, are known to be powerful enough to be considered one of the major hazards in the nuclear power industry [1, 2]. The studies on this phenomenon have been quite active over the past few decades, including the known large-scale experiments FARO [3], KROTOS [4], TROI [5] with the melt masses reaching a hundred kilograms, as well as single-droplet experiments with the melt masses of about one gram [6]–[8]. Despite the significant research effort and progress in the understanding of steam explosion phenomenology, behavior and features, many problems concerning the complex phase interaction still remain unresolved, requiring further experimental, numerical, and analytical studies [9].

It has been established that vapor film instability development plays the leading role in the escalation of heat transfer between the hot melt and cold coolant liquid, resulting in the direct contact of the two fluids, deformation and fragmentation of the molten droplet. The explosive interactions are observed when the melt is superheated high enough above its melting temperature, and water is subcooled with respect to its saturation point. These two conditions ensure that the melt remains liquid during the interaction, and the vapor film is thin enough.

A number of mechanisms for melt droplet fragmentation in the course of interaction has been proposed in the literature. These include the thermal mechanism, related to the capture

of small water droplets by the melt and their subsequent explosive boil-up [10], the fluid dynamics mechanism related to the impact of small-scale water micro-jets on the melt surface causing the splashes of melt [6], as well as other possible mechanisms related to cavitation in the melt caused by pressure wave interactions in the droplet, thermomechanical fragmentation, and others. No single mechanism is capable of explaining all aspects of the interactions observed experimentally, e.g., the material effects, and therefore, this topic still attracts attention from researchers worldwide.

The current work is devoted to numerical modelling of melt-water interaction in the single-droplet configuration. The Volume Of Fluid (VOF) three-dimensional model is applied to the three-phase flow with sharp interfaces. Initially, a spherical molten tin droplet is considered, surrounded by a thin vapor film separating it from the surrounding water. The triggering pressure wave is modelled by a prescribed pressure rise in water, causing the vapor film to collapse and water to impact the melt surface. Thus, the fluid-dynamical mechanism of the interaction is studied, extending the two-dimensional analysis offered in [11], and three-dimensional simulations of jet impact on melt [12] and melt droplet instability [13]. The primary focus of the simulations is on the melt surface perturbations in the course of the interaction, as well as on the details of the melt flow in the droplet caused by the water impact.

2 MATHEMATICAL MODEL

A three-phase system of interacting melt (subscript m), water (w), and vapor (v) is considered. The phases are separated by sharp interfaces, and water evaporation or condensation is taken into account on the water-vapor boundary. In the framework of the Volume Of Fluid (VOF) approach, an effective fluid is introduced where a volume fraction α_k is attributed to each phase. Instead of the actual step-like functions describing the sharp interfaces, smooth distributions of the volume fractions are considered in VOF, but the key point of the method is that the gradients of α_k are maintained as high as possible on the interfaces (therefore, VOF falls into the category of smooth-interface methods, see e.g. [14]). The phase volume fractions α_k satisfy the natural compatibility condition $\alpha_m + \alpha_w + \alpha_v = 1$.

In the VOF approach, common velocity and pressure fields apply to all the phases, whereas the properties of the effective fluid depend on the respective properties of the phases as:

$$\rho = \sum_k \alpha_k \rho_k \,, \quad \rho h = \sum_k \alpha_k \rho_k h_k \,, \quad \eta = \sum_k \alpha_k \eta_k \,, \quad \lambda = \sum_k \alpha_k \lambda_k \tag{1}$$

Here, ρ is the density, h is the specific sensible enthalpy, η is the dynamic viscosity, and λ is the thermal conductivity (the phase properties are denoted by subscript $k = m, w, v$). The flow is described by the following equations expressing the phase continuity, momentum and energy conservation:

$$\frac{\partial \rho_k \alpha_k}{\partial t} + \nabla\left(\rho_k \alpha_k \boldsymbol{U}\right) = \Gamma_k \tag{2}$$

$$\rho \frac{D\boldsymbol{U}}{Dt} = -\nabla P + \nabla \boldsymbol{\tau} + \boldsymbol{F}_\mathrm{s} \tag{3}$$

$$\rho \frac{Dh}{Dt} = \frac{DP}{Dt} + \nabla \lambda \nabla T - \Gamma \Delta h_{ev} \tag{4}$$

Here, t is the time, P and T are the pressure and temperature, $\boldsymbol{U}$ is the velocity vector, Γ_k is the phase change source term ($\Gamma_m = 0$, $-\Gamma_w = \Gamma_v = \Gamma$, where Γ is the water evaporation rate per unit volume), Δh_{ev} is the latent heat of evaporation. The stress tensor is $\boldsymbol{\tau} = \eta\left(\nabla \boldsymbol{U} + \nabla \boldsymbol{U}^T - \frac{2}{3}\boldsymbol{I}\left(\nabla \cdot \boldsymbol{U}\right)\right)$, while the surface tension force $\boldsymbol{F}_{\mathrm{s},k}$ acting on k-th liquid phase $\left(k = m, w\right)$ is described by the continuous surface force (CSF) model [14]:

$$\boldsymbol{F}_{\mathrm{s},k} = \sigma_k \kappa_k \nabla \alpha_k \tag{5}$$

Here, σ_k is the surface tension of k-th liquid on the interface with vapor, and $\kappa_k = -\nabla\left(\nabla \alpha_k / \left|\nabla \alpha_k\right|\right)$ is the surface curvature of k-th liquid. In Eq. (3), the total surface tension force is $\boldsymbol{F}_{\mathrm{s}} = \sum_k \boldsymbol{F}_{\mathrm{s},k}$.

The velocity constraint is obtained by summing up the phase continuity equations (2):

$$\nabla \boldsymbol{U} = -\sum_{k=1}^{K} \frac{\alpha_k}{\rho_k} \frac{D\rho_k}{Dt} + \Gamma\left(\frac{1}{\rho_{\mathrm{v}}} - \frac{1}{\rho_{\mathrm{w}}}\right) \tag{6}$$

The right-hand side of Eq. (6) contains the terms describing the phase compressibility effects (the leftmost term) and dilatation due to evaporation (the rightmost term). The phase volume fraction equations are obtained from (2) in the following form:

$$\frac{\partial \alpha_k}{\partial t} + \left(\boldsymbol{U} \cdot \nabla\right)\alpha_k + \alpha_k\left(\nabla \boldsymbol{U}\right) = -\frac{\alpha_k}{\rho_k}\frac{D\rho_k}{Dt} + \frac{\Gamma_k}{\rho_k} \tag{7}$$

The ideal-gas equation of state is applied to the vapor phase, whereas the liquid phases are described by the linear compressibility model $\left(k = m, w\right)$.

The evaporation rate Γ^+ is described by a model similar to that proposed in [15]:

$$\Gamma^+ = \frac{3\sqrt{2}\lambda_w \left|\nabla \alpha_w\right|}{5\Delta x \Delta h_{ev}} \max(T - T_{sat}, 0) \tag{8}$$

Here, Δx is the cell size, $T_{sat}\left(P\right)$ is the saturation temperature at the local pressure. The condensation rate Γ^- is described by the same formula, with the rightmost factor substituted by $\max(T_{sat} - T, 0)$). Thus, Γ^+ and Γ^- are turned on or off alternatively, depending on whether the local temperature is above or below the saturation temperature. Note that (8) does not involve any problem-specific empirical constants, unlike the widely applied Lee model [16] widely used in simulations with phase change.

Numerical implementation of the mathematical model was performed in the framework of the open-source CFD toolbox OpenFOAM-v1912 [17]. A new VOF solver taking into account both the phase compressibility and phase changes (unavailable in the standard distribution) was developed and implemented. Validation of this solver was performed by solving the test problems (e.g. the Stefan problem on the evaporation front propagation). This solver was also applied successfully in our previous studies on melt-water interactions [12] and [13].

3 GEOMETRY AND PARAMETERS

Vapor film collapse simulation were carried out in a computational domain having the shape of a cube with the side of length $H = 7.32$ mm. Due to the symmetry of the problem,

the domain covered 1/8 of the actual space, see the sketch in figure 1. Simulations were performed on a uniform 125×125×125 mesh. Collapse of the vapor film separating the hot melt and water is caused by the sudden surge of water pressure, which is provided by the corresponding boundary conditions.

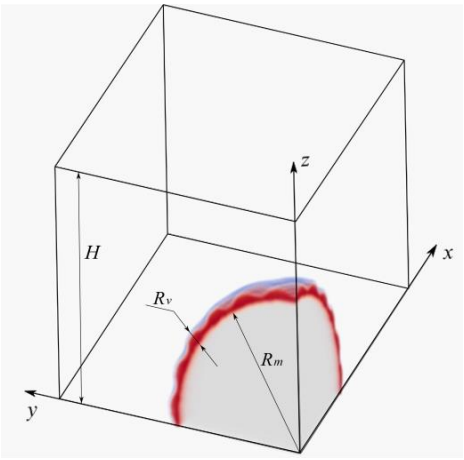

Figure 1: Sketch of computational domain (grey colour denotes melt, red colour is vapour film), 1/8 of the actual domain.

The left, front, and bottom boundaries were considered as symmetry planes. All other boundaries were open, with the boundary pressure varying in time as

$$P_{bnd} = \begin{cases} P_a + (P_0 - P_a)\dfrac{t}{t_d}, & 0 \le t \le t_d \\ P_a + (P_0 - P_a)\exp(-(t - t_d)/t_0) & t \ge t_d \end{cases} \quad (9)$$

Here, $P_a = 1$ bar is the initial pressure in the melt drop and in the vapor film, whereas P_0 is the peak pressure in water which takes a high value of 40 or 80 bars, t_d is the pressure growth time, t_0 is the pressure decay time. For $t_d = 0$, the pressure jumps instantaneously from P_a to P_0 (shock wave), otherwise it linearly grows to its maximum value and then decays exponentially. These pressure boundary conditions imitate the arrival of a pressure wave propagating in water.

The droplet material was molten tin, a metal with a relatively low melting point, often used in experiments on fuel-coolant interaction (see e.g., [6] and [7]). The properties of tin were taken from [18]; along with the properties of other phases, they are summarized in table 1.

Table 1: Phase properties

Property / Phase	Density, kg/m^3	Specific heat capacity, J/(kg·K)	Dynamic viscosity, Pa·s	Conductivity, W/(m·K)	Surface tension, N/m
Melt	6689	263	$0.9\cdot10^{-3}$	38.4	0.52
Water	1027	4181	$0.3\cdot10^{-3}$	0.65	0.06
Vapor	changing	1800	$3.5\cdot10^{-5}$	0.09	0.06

Initially, the melt drop radius was $R_m = 3.36$ mm, the average thickness of the vapor film was $R_v = 0.5$ mm; and the rest of the space was filled with subcooled water. The initial temperatures of melt, water and vapor were $T_{\mathrm{m}} = 950$ K, $T_w = 323\,\mathrm{K}$ and $T_{\mathrm{v}} = 373$ K (saturated vapor), respectively. The water-vapor interface was perturbed by creating several spherical water bulges facing towards the melt droplet.

4 RESULTS

To study the evolution of vapor film and melt droplet during the melt-water interaction initiated by ambient pressure growth, simulations were carried out for the cases listed in table 2.

Table 2: Simulation cases

Case	Initial pressure P_0, MPa	Time constant t_0, μs	Pressure growth time t_d, μs
C1	8	100	0
C2	8	30	0
C3	4	100	0
C4	4	30	0
C5	8	70	0
C6	8	30	20
C7	8	30	80

The first five cases (C1–C5) correspond to different intensity and pressure decay rate in the arriving shock, and the details of interaction in cases C1-C4 were presented elsewhere [13]. In figure 2, the three-dimensional melt droplet shapes corresponding to case C2 are shown, demonstrating the development of significant splashes on the melt surface. It was shown that rapid decay of the ambient pressure (cases C2 and C4) led to occurrence of only a single bubble oscillation, whereas in cases C1 and C3 three bubble oscillations were observed. Case C5 corresponds to the boundary where two bubble oscillations occurred.

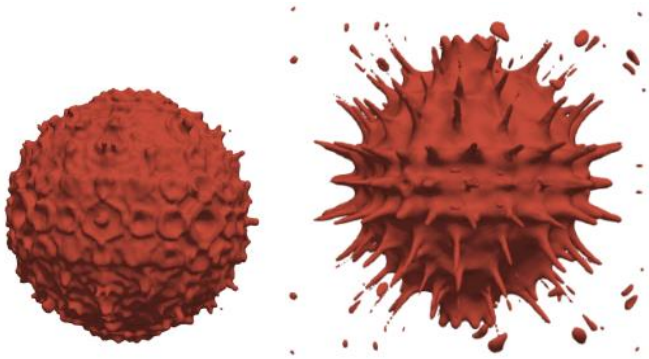

Figure 2: Melt droplet surface at times 100 (left) and 400 μs (right), case C2

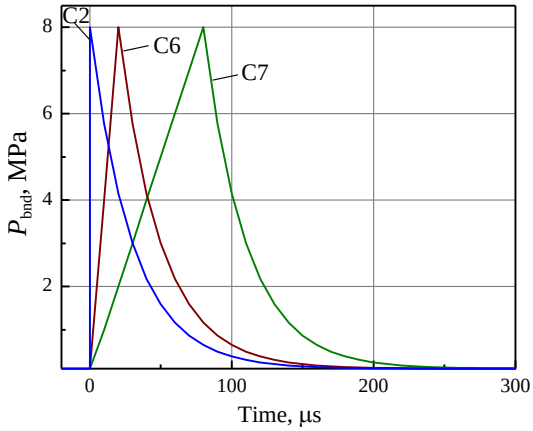

Figure 3: Pressure changes for cases C2, C6 and C7

The instantaneous pressure jump in the cases C1–C5 is an idealization, in the actual interactions more gradual pressure growth can be expected due to finite-duration triggering. In order to analyze the effects of pressure pulse shape on the melt-water interaction, cases C6 and C7 were considered which have the parameters equivalent to case C2, except for the different pressure growth times t_d, see table 1. The respective ambient pressure histories are plotted in figure 3.

In figure 4, the interaction of melt droplet with water is shown for the case C6, with parameters of case C2: initial water pressure of 8 MPa and the pressure decay time of 30 μs, but with linear rise of pressure over time $t_d = 20$ μs. The distributions of volume fractions are shown in the vertical plane of symmetry $y = 0$ at five consecutive instants $t = 20,\ 30,\ 100,$ 200, and 400 μs, with white color denoting melt, red color corresponding to vapor, and blue color denoting water. Due to the presence of pressure growth stage, the first collapse of vapor film occurs by the time 30 μs which exceeds the corresponding time for the base case C2. Then, the second impact of water on the melt occurs by the time 100 μs. The melt surface becomes significantly perturbed in the course of interaction due to the impacts of water jets. In the contact zone, pressure surges caused by the water impact along with rapid evaporation are obtained; vapor expansion is clearly visible on the frames at times of 100–400 μs.

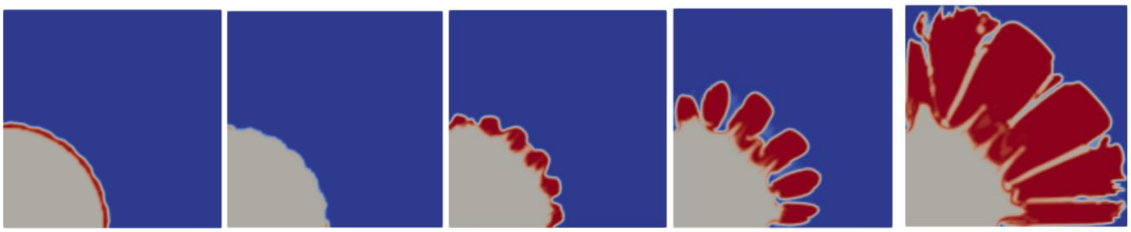

Figure 4: Melt droplet interaction with water at times of 20, 30, 100, 200, and 400 μs (left to right), case C6.

Water jet impact and evaporation cause the development of internal melt flows in the droplet. This is demonstrated in figure 5 where distributions of volume fractions in the planes of symmetry $x = 0$ and $y = 0$ are presented. The development of flows inside the melt and vapor film can be described by the following sequence: the impact of water jets on a vapor film leads to its collapse and further direct contact of water with the melt, which leads to rapid expansion of vapor and the appearance of melt splashes. The analysis shows that the positions of melt splashes correspond to the points of the first contact of water with melt; therefore, the

splashes which are observed at time 150 μs are similar to the known cumulative jets caused by the impact of water on the melt surface (see the recent experimental results [19]).

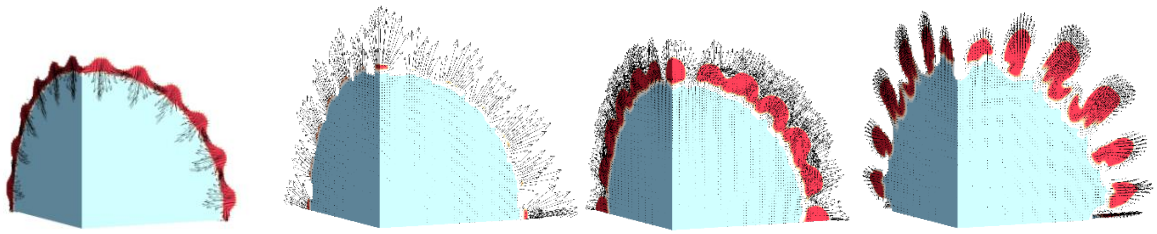

Figure 5: Flows in melt droplet and vapor film at times of 14, 32, 50 and 150 μs (left to right), case C6

To characterize the amount of vapor surrounding the melt droplet, the instantaneous total volume of vapor was calculated and plotted against time. Figure 6a shows the calculated volumes of vapor for cases C1-C5, indicating that the number of vapor film oscillations is dependent upon the rate of pressure decay. The calculated volumes of vapor for cases C2, C6, and C7 are also plotted in figure 6b. It can be seen that for the longer pressure growth time (case C7) the bubble oscillates 2 times in the course of interaction, while in the cases of instantaneous pressure growth (C2) and shorter pressure growth (C6) only a single oscillation occurs. However, as it was discussed above, in the case C6 a secondary impact of water occurs at time 100 μs, not reflected on the vapor volume curve because water penetrates through the vapor film as thin jets, without complete collapse of vapor. These results suggest that it is important to consider, in the simulations and comparisons with experiments, the shape of pressure peak pulse, because it can affect the interactions between water and melt significantly.

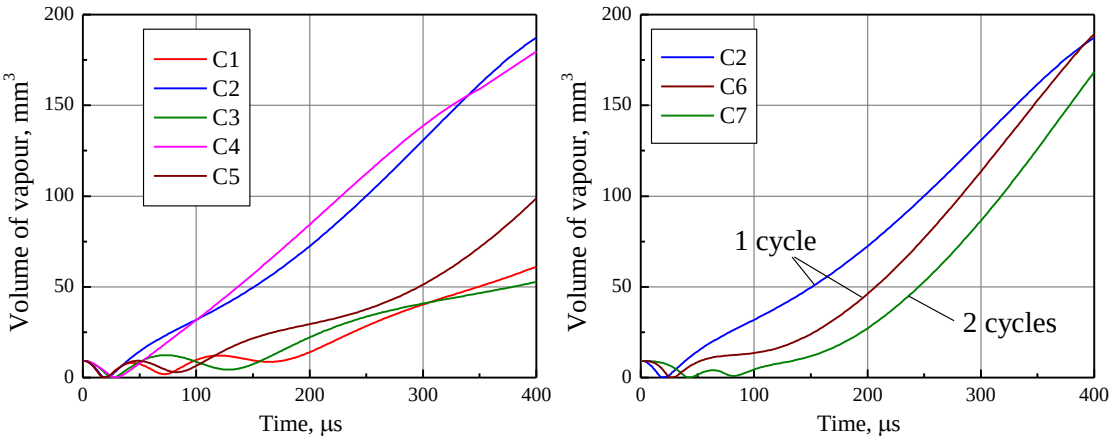

a) b)

Figure 6: Vapor volume time histories in cases C1–C7

5 CONCLUSIONS

The studies performed in this work by VOF method were focused on the interaction of a single melt droplet with water. The difference from previous works consists in the study of the dependence of the process of collapse of the vapor film on the initial increase in pressure in the region of interaction. In the course of the study, it was revealed that the rate of pressure growth can lead to the appearance of additional oscillations of the vapor film, which will lead

to additional direct contacts of water with the melt, followed by fragmentation of the melt and the formation of splashes of the melt. In the further studies, it is worthwhile to consider more thoroughly the influence of the parameters of the pressure wave (triggering), in particular, to vary the dependences of pressure with its initial increase and further decay.

The results obtained in this work are qualitatively consistent with the experimental observations on single-droplet steam explosions presented in [6]. In particular, the initial stages of the interaction are observed, including the vapor bubble collapse, formation of multiple melt spikes, followed by the secondary bubble collapse increasing the melt perturbation amplitude. Although in the simulations some fine fragmentation of melt was observed (visible as fine droplets detached from the melt droplets and braids), no bulk fragmentation of the droplet was obtained (note that similar results were obtained in 2D simulations [11]). This means that more complex models of interaction must be invoked in addition to the hydrodynamic interaction model used in the current work.

Quantitative validation of VOF simulations will be performed in the future; it requires calculations in proper geometry and conditions corresponding to the experiments. Such studies will also allow the requirements to numerical grid resolution to be established.

ACKNOWLEDGMENTS

This research was funded by Russian Science Foundation (RSF) under Grant 18-19-00289.

REFERENCES

[1] G. Berthoud, “Vapor Explosions”, Annu. Rev. Fluid Mech., 32, 2000, pp. 573–611.
[2] V.I. Melikhov, O.I. Melikhov, S.E. Yakush, Fluid Mechanics and Thermal Physics of Steam Explosions, IPMech RAS, Moscow, 2020. [In Russian]
[3] D. Magallon, I. Huhtiniemi, “Corium Melt Quenching Tests at Low Pressure and Subcooled Water in FARO”. Nucl. Eng. Des., 204, 2001, pp. 369–376.
[4] I. Huhtiniemi, D. Magallon, “Insight into Steam Explosions with Corium Melts in KROTOS,” Nucl. Eng. Des., 204, 2001, pp. 391–400.
[5] J.-H. Kim, I.-K. Park, S.-W. Hong, B.-T. Min, S.-H. Hong, J.-H. Song, H.-D. Kim, “Steam Explosion Experiments Using Nuclear Reactor Materials in the TROI Facilities”, Heat Transf. Eng., 29, 2008, pp. 748–756.
[6] G. Ciccarelli, D.L. Frost, “Fragmentation Mechanisms Based on Single Drop Steam Explosion Experiments Using Flash X-ray Radiography”, Nucl. Eng. Des., 146, 1994, pp. 109–132.
[7] R. C. Hansson, H. S. Park, T.-N. Dinh, “Simultaneous High Speed Digital Cinematographic and X-ray Radiographic Imaging of a Intense Multi-fluid Interaction with Rapid Phase Changes”, Exp. Therm. Fluid Sci., 33, 2009, pp. 754–763.
[8] L. Manickam, G. Qiang, W. Ma, S. Bechta, “An Experimental Study on the Intense Heat Transfer and Phase Change during Melt and Water Interactions”, Exp. Heat Transf., 32, 2019, pp. 251–266.
[9] R. Meignen, B. Raverdy, M. Buck, G. Pohlner, P. Kudinov, W. Ma, C. Brayer, P. Piluso, S-W. Hong, M. Leskovar, M. Uršič, G. Albrecht, I. Lindholm, I. Ivanov, “Status of Steam Explosion Understanding and Modelling”, Ann. Nucl. Energy, 74, 2014, pp. 125–133.
[10] B. Kim, M.L. Corradini, “Modeling of Small-Scale Single Droplet Fuel/Coolant Interactions”, Nucl. Sci. Eng. 98, 1988, pp. 16–28.

[11] Y. Zhou, Z. Zhang, M. Lin, Y. Minghao, Y. Xiao, “Numerical Simulation of Fragmentation of Melt Drop Triggered by External Pressure Pulse in Vapor Explosions” Ann. Nucl. Energy, 57, 2013, pp. 92–99.
[12] S. E. Yakush, N. S. Sivakov, V. I. Melikhov, O. I. Melikhov, “Hot Melt Splash upon Impingement of a Water Jet”, J. Phys. Conf. Ser., 1666, 2020, paper 012060.
[13] S. E. Yakush, N. S. Sivakov, V. I. Melikhov, O. I. Melikhov, “Numerical Modelling of Melt Droplet Interaction with Water”, J. Phys. Conf. Ser., 2021 [In print]
[14] G. Tryggvason, R. Scardovelli, S. Zaleski, “Direct Numerical Simulations of Gas-Liquid Multiphase Flow”, Cambridge University Press, Cambridge MA, 2011.
[15] G. Chen, T. Nie, X. Yan, “An Explicit Expression of the Empirical Factor in a Widely Used Phase Change Model”, Int. J. Heat Mass Transf., 150, 2020, paper 119279.
[16] W. H. Lee, “A pressure iteration scheme for two-phase modeling. Technical Report LA-UR 79-975”, Los Alamos Scientific Laboratory, Los Alamos, New Mexico, 1979.
[17] OpenFOAM. The open source CFD toolbox 2012 URL: https://www.openfoam.com
[18] Y. Plevachuk, V. Sklyarchuk, G. Gerbeth, S. Eckert, R. Novakovic, “Surface Tension and Density of Liquid Bi–Pb, Bi–Sn and Bi–Pb–Sn Eutectic Alloys”, Surf. Sci., 605, 2011, pp. 1034–1042.
[19] S.E. Yakush, Y.D. Chashechkin, A.Y. Ilinykh, V.A. Usanov, “The Splashing of Melt upon the Impact of Water Droplets and Jets”, Appl. Sci. 11 909, 2021.